Acetylene Chemistry

Chemistry, Biology and Material Science

Edited by
F. Diederich, P. J. Stang, R. R. Tykwinski

WILEY-VCH Verlag GmbH & Co. KGaA

Acetylene Chemistry

Edited by
F. Diederich, P. J. Stang,
R. R. Tykwinski

Further Reading from Wiley-VCH

A. de Meijere, F. Diederich (Eds.)
Metal-Catalyzed Cross-Coupling Reactions, 2nd Ed., 2 Vols.
2004, ISBN 3-527-30518-1

R. Mahrwald (Ed.)
Modern Aldol Reactions, 2 Vols.
2004, ISBN 3-527-30714-1

N. Krause, A. S. K. Hashmi (Eds.)
Modern Allene Chemistry, 2 Vols.
2004, ISBN 3-527-30671-4

R. Gleiter, H. Hopf (Eds.)
Modern Cyclophane Chemistry
2004, ISBN 3-527-30713-3

Acetylene Chemistry

Chemistry, Biology and Material Science

Edited by
F. Diederich, P. J. Stang, R. R. Tykwinski

WILEY-VCH Verlag GmbH & Co. KGaA

Editors:

Prof. Dr. François Diederich
Laboratorium für Organische Chemie
ETH Hönggerberg, HCI
CH-8093 Zürich
Switzerland

Prof. Dr. Peter J. Stang
Department of Chemistry
University of Utah
315S 1400E, Rm. 2020
84112 Salt Lake City
USA

Prof. Dr. Rik R. Tykwinski
Department of Chemistry
University of Alberta
T6G 2G2 Edmonton
Canada

Library of Congress Card No.: applied for
British Library Cataloguing-in-Publication Data:
A catalogue record for this book is available from the British Library.

Bibliographic information published by Die Deutsche Bibliothek
Die Deutsche Bibliothek lists this publication in the Deutsche Nationalbibliografie; detailed bibliographic data is available in the Internet at <http://dnb.ddb.de>.

Printed in the Federal Republic of Germany.
Printed on acid-free paper.

Typesetting hagedorn kommunikation, Viernheim
Printing betz-druck gmbh, Darmstadt
Bookbinding Litges & Dopf Buchbinderei GmbH, Heppenheim

ISBN 3-527-30781-8

Preface

The carbon-carbon triple bond is a common structural motif in organic chemistry. Only during the past two decades, however, has it become a mainstay in the toolbox of synthetic organic chemists, biochemists, and materials scientists. Both as a building block and as a versatile synthon, the fascinating and sometimes unpredictable chemistry associated with the alkyne moiety has fueled many of the most recent advances. A decade ago, the monograph *Modern Acetylene Chemistry* documented an emerging renaissance in the chemistry of the carbon-carbon triple bond. Over the past ten years, this renaissance has evolved at an astounding rate and acetylenes now constitute a principal class of compounds in nearly all areas of chemistry and materials science.

The explosive growth of acetylene chemistry has particularly benefited from the development of new synthetic methodology based on transition metal catalysts and metal acetylides. An acetylene unit can now be introduced into nearly any desired molecule, large or small, often with surprising ease. Metal acetylides are key components for generating new nucleophilic reagents suitable for asymmetric addition reactions into electrophilic multiple bonds. The chemistry of early transition metal acetylides is especially rich, providing a fascinating class of compounds with remarkable synthetic potential. Acetylene chemistry has also driven the development of new methodology such as electrophilic addition reactions that allow the derivatization of this high-energy functional group into hetero- and carbocycles of significant interest to both synthetic and medicinal chemists. Alkynes are also versatile synthetic building blocks for the formation of natural product analogues and hybrid structures. For example, combining the hydrophobic, rigid, and linear attributes of acetylenes with the hydrophilic and chiral framework of carbohydrates affords derivatives with interesting structural properties and biological activity.

The advent of fullerene and nanotube chemistry in the 1990s inspired the search for other molecular carbon allotropes, and the hunt for both linear and cyclic allotropes consisting of sp–hybridized carbon continues in earnest. The study of carbon clusters, both linear and cyclic, spans from astrophysics to fullerene formation and advances in synthetic methodology are propelling efforts on all fronts. Acetylenic carbon rings can now be generated in the gas phase by a number of routes, while acyclic polyynes with lengths of several nanometers can be produced in unprecedented quantities with a range of terminal appendages. Cleverly designed acetylenic scaffolds can also serve as precursors to carbon-rich structures such as fullerenes and bucky onions. These recent discoveries provide for the tantalizing possibility of designer fullerenes with engineered shape and size.

Structural rigidity and electronic communication which is essentially unperturbed by conformational effects are the hallmarks of the acetylene moiety. These attributes make it a highly versatile component for conjugated scaffolds, especially when coupled with the extraordinary advances that have been achieved in metal catalyzed cross-coupling reactions. Nowhere is this more evident than in the spectacular array of molecules that have been assembled based on an arylene ethynylene framework. The synthesis of macrocycles based on arylacetylenes has now evolved to the point where constitution, physical properties, and chemical reactivity can be controlled in exquisite detail. Many of these molecules have been structurally tailored to exhibit specific properties of use in semiconductors, nonlinear optical media, liquid crystals, and sensors. Shape persistent acetylenic macrocycles can provide ordered systems based both on super- and supramolecular chemistry, resulting in tubular superstructures, two-dimensional networks, hosts for molecular recognition, and even adaptable systems that conform to external stimuli. Oligomeric, dendrimeric, and polymeric systems based on arylene ethynylene subunits are now widely viewed as some of the most important semiconducting organic materials. Vital to the successful application of these materials is the development of a much more thorough understanding of the key aspects of their synthesis, electronic structure, and organization into well-ordered films. The fruits of these efforts include synthetic polymers with programmed solid-state organization and ultra-sensitive molecular sensors for TNT. Arylene ethynylene structures incorporating chiral 1,1'-binaphthyl subunits provide yet another appealing dimension to these materials, and optically active acetylenic scaffolds suitable for asymmetric catalysis, nonlinear optics, and polarized emission have all been realized.

Complementing the efforts of synthetic and experimental chemists are the substantial achievements of theoretical chemists in their ability to both model and predict the properties of acetylene-rich molecules. The ever-increasing power of computational hardware, coupled with the development of new and improved numerical methods, have made theoretical modeling a vital tool in the evolution of modern acetylene chemistry. These efforts have shed light on topics ranging from the fundamentals of homoconjugation to the prospect of utilizing acetylene-based molecular wires as components in molecular electronics.

The eleven expert authors that have contributed to this monograph collectively offer a rich overview of the modern face of acetylene chemistry, as well as a detailed analysis of more subtle aspects that can dictate the success or failure of a particular experiment. Considerable emphasis has been placed on outlining the most recent advances in key areas of this discipline. We hope that this monograph offers to the novice a taste of the fundamental issues that motivate this exciting field of science, and to the expert the specific details on synthesis and applications necessary to stimulate the future of acetylene chemistry.

The editors wish to thank Dr. Elke Maase at Wiley-VCH for an enjoyable collaboration in the preparation of this book and Ms. Annie Tykwinski for designing the cover art.

November, 2004 F. Diederich, P. J. Stang, R. R. Tykwinski

Contents

Symbols and Abbreviations

A	adenine
ABLA	absolute bond length alternation parameter
Ac	acetyl
ADF	Amsterdam density functional
AFM	atomic force microscopy
AIBN	azobis(isobutyronitrile)
AIM	atoms in molecules
All	allyl
AM1	Austin model 1
APCI	atmospheric pressure chemical ionization
ARCS	aromatic ring current shielding
ASE	aromatic stabilization energy
ATRP	atom transfer radical polymerization
B3LYP	hybrid funtional by Becke and Lee-Yang-Parr
B3PW91	hybrid functional by Becke and Perdew-Wang
BHT	3,5-di-*tert*-butyl-4-hydroxytoluene
BINOL	1,1′-binaphthalene-2,2′-diol
BLYP	Bekce/Lee-Yang-Parr functional
bmim	1-butyl-3-methylimidazolium
Bn	benzyl
Boc	*tert*-butoxycarbonyl
BPO	benzoyl peroxide
bpy	2,2′-bipyridyl
BRE	Breslow resonance energy
BTEACl	benzyltriethylammonium chloride
$BTEAICl_2$	benzyltriethylammonium dichloroiodate
$BTEAICl_3$	benzyltrimethylammonium tribromide
BTMSA	bis(trimethylsilyl)acetylene
$BTMABr_3$	benzyltrimethylammonium tribromide
Bu	butyl
BuLi	butyllithium
Bz	benzoyl

CAN	ceric ammonium nitrate
CASSCF	complete active-space self consistent field
CC	coupled cluster
CCSDT/ CCSD(T)	coupled cluster singles doubles triples
CD	circular dichroism
CNDO/S-CI	complete neglect differential orbital/singles configuration interaction
COD	1,5-cyclooctadiene
Cp	cyclopentadienyl
Cp′	differently substituted cyclopentadienyl
Cp^*	pentamethylcyclopentadienyl
CPDMS	3-cyanopropyldimethylsilyl
CRD	cavity ring-down (spectroscopy)
CSA	camphorsulfonic acid
$<d>$	average diameter
DABCO	1,4-diazabicyclo[2.2.2]octane
dba	dibenzylideneacetone
DBU	1,8-diazabicyclo[5.4.0]undec-7-ene
DCC	dicyclohexylcarbodiimide
DCE	1,2-dichloroethane
DE	dissociation energy
DEAD	diethyl azodicarboxylate
Dec	decyl
DET	diethyl tartrate
DFT	density functional theory
"D+G" band	"disorder-induced" + "graphite" band
DIB	diffuse interstellar band
DIBAH	diisobutylaluminium hydride
DIC	*N,N′*-diisopropylcarbodiimide
DL	diode laser
DLS	dynamic light scattering
DMAP	4-dimethylaminopyridine
DME	1,2-dimethoxyethane
DMF	*N,N*-dimethylformamide
DMI	1,3-dimethyl-2-imidazolidinone
DMSO	dimethylsulfoxide
Dod	dodecyl
DOKE	differential optical Kerr effect
DOPS-TIPS	$SiMe_2CMe_2CH_2CH_2OSi(CHMe_2)_3$
DP	degree of polymerization
dppe	1,2-bis(diphenylphosphino)ethane
dppp	1,3-bis(diphenylphosphino)propane
DSC	differential scanning calorimetry

EA	electron affinity
ebthi	ethylene-bis-tetrahydroindenyl
ED	electron diffraction
EDX	energy dispersed X-ray emission
ee	enantiomeric excess
EELS	electron energy loss spectroscopy
EEM	electronegativity equalization method
ELF	electron localization function
E_{max}	energy of maximum absorption
EP	ethynylphenylene
EPR	electron paramagnetic resonance
equiv	equivalents
esu	electrostatic unit
Et	ethyl
FBW	Fritsch-Buttenberg-Wiechell
FC	flash chromatography
fs	femtosecond
fur	furyl
FVP	flash vacuum pyrolysis
FWHM	full width at half maximum
γ	molecular second hyperpolarizability
Gal	galactose
GGA	gradient generalized affroximation
Glc	glucose
GPC	gel permeation chromatography
hν	light
Hep	heptyl
Hex	hexyl
HF	Hartree-Fock
HMPA	hexamethylphosphoramide
HOMO	highest occupied molecular orbital
HOPG	highly oriented pyrolytic graphite
ICR	ion cyclotron resonance
INDO	intermediate neglect differential orbital
IP	ionization potential
K_{assoc}	association constant
l	contour length
λ_{max}	wavelength of maximum absorption
LB	Langmuir–Blodgett

LC	liquid crystal
LDA	lithium diisopropylamide
LD-TOF	laser desorption time of flight
LE	locally excited
LLS	laser light scattering
LiHMDS	lithium hexamethyldisilazide
LUMO	lowest unoccupied molecular orbital
MALDI-TOF	matrix-assisted laser desorption/ionization time-of-flight
Me	methyl
MINDO	modified intermediate neglect differntial orbital
min	minutes
MMC	molecular mechanics for clusters
MM3	molecular mechanics 3
M_n	number average molecular weight
MNDO/3	modified neglect differential orbital number 3
MOM	methoxymethyl
MP2, MP4	Moller Plesset 2, Moller Plesset 4
MRD-CI	multi-reference single and doubly excitation configuration
MRTD	molecular resonant tunneling diode
Ms	mesyl
M_w	weight average molecular weight
NBO	natural bond order
NBS	*N*-bromosuccinimide
NCS	*N*-chlorosuccinimide
NDR	negative differential resistance
NICS	nucleus independant chemical shift
NIS	*N*-iodosuccinimide
NLO	nonlinear optics
NLP	nonlinearity parameter
NME	*N*-methylephedrine
NMO	*N*-methylmorpholine *N*-oxide
NMP	*N*-methyl-2-pyrrolidone
ns	nanosecond
Oct	octyl
ODCB	*ortho*-dichlorobenzene
ODf	difluoromethanesulfonate
OEP	oligoethynylphenylene
OITB	orbital interaction through bonds
OITS	orbital interaction through space
ORTEP	Oak Ridge thermal ellipsoid plot
OTf	trifluoromethanesulfonate

PArE	poly(arylene ethynylene)
PAM	phenylacetylene macrocycle
PCC	pyridinium chlorochromate
PDI	polydispersity index
PDM	phenyldiacetylene macrocycle
PM3	parametric method number 3
PDA	poly(diacetylene)
Ph	phenyl
PhLi	phenyllithium
PHT	phenylheptatriyne
Pic	picrate
Piv	pivaloyl (*tert*-butylcarbonyl)
PmB	*para*-methoxybenzyl
PPE	poly(phenylene ethynylene)
PPV	poly(phenylene vinylene)
Pr	propyl
PS	polystyrene
PTA	poly(triacetylene)
PTFE	polytetrafluoroethylene
PTeM	phenyltetraacetylene macrocycle
PTrM	phenyltriacetylene macrocycle
py	pyridine
QUINAP	1-(2-diphenylphosphanyl-naphthalen-1-yl)-isoquinoline
R2CPD	resonance two-color photodetachment
REMPED	resonance-enhanced multi-photon detachment
RHF	restricted Hartree-Fock
rt	room temperature
SAM	self-assembled monolayer
SCF	self consistent field
SERS	surface plasmon polariton-enhanced Raman spectra
SHG	second harmonic generation
SSH	Su-Schrieffer-Heeger
STM	scanning tunneling microscopy
STO-3G	minimal Pole basis set
T	thymine
TBAF	tetrabutylammonium fluoride
TBDMS	*tert*-butyldimethylsilyl
TBS	*tert*-butyldimethylsilyl
TCNQ	7,7,8,8-tetracyanoquinodimethane
TD	Time dependent
TDDFT	time-dependent DFT

TEBAC	triethylbenzylammonium chloride
TEE	tetraethynyl-ethylene
TEM	transmission electron microscopy
Tf	trifluoromethanesulfonyl
TFA	2,2,2-trifluoroacetic acid
TGA	thermal gravimetric analysis
Th	Thexyl, 1,1,2-trimethylpropyl
THF	tetrahydrofuran
THP	tetrahydropyranyl
TIPS	triisopropylsilyl
TIPSA	triisopropylsilylacetylene
TLC	thin layer chromatography
TMEDA	*N,N,N′,N′*-tetramethylethylenediamine
TMS	trimethylsilyl
TMSA	trimethylsilylacetylene
TMU	tetramethylurea
TNT	trinitrotoluene
TOF-MS	time-of-flight mass spectrometry
Tol	4-tolyl (4-methylphenyl)
Ts	*p*-toluenesulfonyl
Tr	trityl (triphenylmethyl)
U	uracil
UPS	ultraviolet photoelectron spectroscopy
VEH/SOS	valence effective Hamiltonien/sum over states
VSEPR	valence shell electron pair repulsion
VPO	vapor pressure osmometry
VUV	vacuum UV
ZINDO	Zerner intermediate neglect differential overlap

List of Contributors

Patrick Aschwanden
Laboratorium für Organische Chemie
ETH Zürich
8093 Zürich
Switzerland

Bruno Bernet
Laboratorium für Organische Chemie
ETH Zürich
8093 Zürich
Switzerland

Erick M. Carreira
Laboratory of Organic Chemistry
ETH Hoenggerberg, HCI
8093 Zürich
Switzerland

Rémi Chauvin
CNRS
Laboraoire de Chimie de Coordination
205 Route Narbonne
31077 Toulouse, Cedex 4
France

Sara Eisler
Department of Chemistry
University of Alberta
Edmonton, Alberta
T6G 2G2
Canada

Michael M. Haley
Department of Chemistry
1253 University of Oregon
Eugene, Oregon 97403-1253
USA

Carissa S. Jones
Department of Chemistry
and the Materials Science Institute
1253 University of Oregon
Eugene, Oregon 97403-1253
USA

Sigurd Höger
Polymer Institut
Universität Karlsruhe
Hertzstraße 16
76187 Karlsruhe
Germany

Richard C. Larock
Department of Chemistry
1605 Gilman Hall
Iowa State University
Ames, IA 50011-3111
USA

Christine Lepetit
CNRS
Laboraoire de Chimie de Coordination
205 Route Narbonne
31077 Toulouse, Cedex 4
France

Matthew J. O'Connor
Department of Chemistry
and the Materials Science Institut
1253 University of Oregon
Eugene, Oregon 97403-1253
USA

Lin Pu
Department of Chemistry
Universtiy of Virginia
PO Box 400319
Charlottesville, VA 22904-4319
USA

Uwe Rosenthal
Institut für Organische
Katalyseforschung
Universität Rostock e.V.
Buchbinderstraße 5–6
18055 Rostock
Germany

Timothy M. Swager
Department of Chemistry
Massachusetts Institute of Technolgoy
77 Massachusetts Ave.
Cambridge, MA 02139
USA

Yoshito Tobe
Department of Chemistry
Faculty of Engineering Science
Osaka University
Toyonaka, Osaka 560-8531
Japan

Rik R. Tykwinski
Department of Chemistry
University of Alberta
Edmonton, Alberta
T6G 2G2
Canada

Andrea Vasella
Laboratory of Organic Chemistry
ETH Hoenggerberg, HCI
8093 Zürich
Switzerland

Tomonari Wakabayashi
Department of Chemistry,
School of Science and Engineering
Kinki University
Higashi-Osaka 557-8502
Japan

1
Theoretical Studies on Acetylenic Scaffolds

Remi Chauvin and Christine Lepetit

1.1
Introduction

Ten years ago, Houk demonstrated that along with experimental analysis, theoretical analysis could not be ignored for advanced understanding of the specific properties of acetylenic compounds [1]. In recent years, the growing power of computational facilities, the optimized implementation of performant methods in various software packages, and the development of new theoretical tools (faster and extended coupled cluster (CC) methods, new density functional theory (DFT) functionals, time-dependent DFT (TDDFT), advanced topological treatments of the information contained in the electron density through the atoms in molecules (AIM) [2], and electron localization function (ELF) [3] methods,…) prompted more and more chemists to consider theoretical modeling as a key tool. This tool is used at either of two levels: (i) a posteriori, for analysis of the properties of known compounds, or (ii) a priori, for selection of synthetic targets with specific properties among potential molecular structures suggested by empirical laws governing the chemist's intuition. This intuition is formally sustained by more systematic suggestion tools, such as the "analogy principle" (variation of some structural unit through structural units with the same valence, such as a terminal atom through all the halogens), the "vinylogy", "cumulogy", or "ethynylogy" principles (insertion of CH=CH, C=C, or C≡C units between a few pairs of conjugated atoms), or the "*carbo*-mer principle" (insertion of C_{sp}-C_{sp} units into at least all symmetry-related bonds of a Lewis structure (Scheme 1.1)) [4]. The last of these principles allows for fine-tuning of the notion of carbon-*rich* molecules [5] to a notion of carbon-

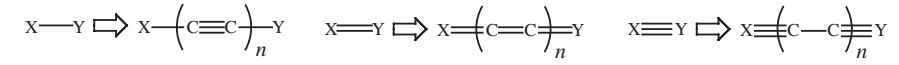

Scheme 1.1 Acetylenic expansions, becoming *carbo*-meric expansions if applied to complete sets of symmetry-related bonds of a parent molecule [4].

enriched molecules: indeed, *carbo*-merization does not corrupt the personality of a parent molecule "too much", as it preserves many of its basic features (connectivity, symmetry, shape, π-electron resonance, CIP configuration of asymmetric centers, …), while just expanding its size through its acetylenic content.

A natural question concerns the variation of pre-existing or emerging properties as a function of the acetylenic content. Theoretical modeling allows for systematic screening and targeting prior to the undertaking of possibly tedious experimental syntheses. It should be emphasized, however, that many constructed expanded acetylenic scaffolds intentionally contain butadiynyl units (C_4) and are quite symmetrical. This holds to the efficiency and variety of oxidative C_{sp}-C_{sp} coupling procedures from terminal alkynes, which also motivated theoretical investigations of their mechanism [6].

This chapter presents selected advances (with special emphasis on results published since 1995) in the theoretical analysis or prediction of the properties of acetylenic scaffolds in a sequence based on dimensionality [7]:

1.2 Linear acetylenic scaffolds
1.3 Cyclic acetylenic scaffolds
1.4 Star-shaped acetylenic scaffolds
1.5 Cage acetylenic scaffolds

1.2 Linear Acetylenic Scaffolds

1.2.1 The Dicarbon Molecule and Acetylene

The empirically observed statistical even/odd carbon atom disparity in organic molecules [8] can be arithmetically interpreted by saying that the latter are made of "carbon pairs" rather than of carbon atoms. The bonded carbon pair, C_2, is the unitary "brick" of acetylenic scaffolds. This molecule can be observed in the form of the blue light of hot hydrocarbon flames [9] (e. g., during the pyrolysis of acetylene itself [10]), but also occurs under various conditions (diamond vapor deposition, laser ablation of graphite, in carbon-rich stars and comets…), and it was quickly proposed that it might assemble into the C_{60} fullerene [11]. The MO diagram of the $^1\Sigma_g^+$ ground state corresponds to the $(2\sigma_g)^2(2\sigma_u)^2(1\pi_u)^4$ configuration, and is nearly degenerate with the first triplet state ($^3\Pi_u$). For the $^1\Sigma_g^+$ state, the simplest orbital criterion (six bonding and two anti-bonding electrons) corresponds to the :C=C: description. Higher bond orders (approximately 3.7) were, however, assigned by Wiberg or natural population analysis (NPA) [12], in accordance with the experimentally determined bond length (1.242 Å) and harmonic frequency (1855.0 cm^{-1}) [13], which are well reproduced by CCSDT methods and non-iterative approximation thereof [14]. The bond is indeed shorter than more stable C_{sp}=C_{sp} double bonds (e. g., approximately 1.280 Å for butatriene at various experimental and theoretical levels [15]). The $^1\Sigma_g^+$ state was thus depicted as a resonance hybrid

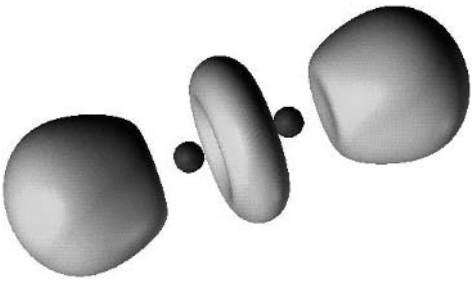

Figure 1.1 Localization domains of the acetylene molecule (ELF = 0.8) [3a]. The two red basins represent the carbon inner shells; the two blue ones the C−H bonds, and the green torus the C≡C bond.

:C=C:↔:C⊙C·↔·C⊙C:, as derived from Feynman's diagrams [16]. If the formal C≡C octet form is excluded [12], the classical Lewis resonance accounting both for the spin state and for the bond length of the $^1\Sigma_g^+$ state would be: :C=C:↔$^+$C≡C:$^-$↔$^-$:C≡C$^+$. Similarly, a consistent picture for the $^3\Pi_u$ state would be ·:C–C:·↔·C≡C·. These pictures suggest that the C_2 units might efficiently transmit π electron delocalization (vide infra).

In unstrained bonding situations, the biscarbenic character of the C_2 unit disappears. In acetylene, for example, the chemical shape of the three-bond rod can be visualized through the ELF localization domains (Figure 1.1) [3a]. According to the axial symmetry of the molecule, the three bond domains expected for the triple C-C bond are degenerate and merged into a torus: there is no σ/π separation, in variance with the classical view of organic chemists.

1.2.2
Uncapped pure *sp* Carbon Chains [1]

Many theoretical studies of all-*sp* carbon clusters C_n show that the open linear form is preferred over the cyclic form for $n < 10$, though cyclic forms of short *n*-even chains (C_4, C_6, C_8) do compete [17]. The converse holds for $n \geq 10$ (see Section 1.3.2.4), but open chains are known for odd n = 3–29 [18].

Optimized geometries at various level of theory indicate that the octet deficiency of carbon chains is partly made up by a strong cumulenic character both for C_{2m+1} chains ($^1\Sigma_g^+$ ground state with equal bond lengths of approximately 1.30 Å) and for C_{2m} chains ($^3\Sigma_g^-$ ground state with less than 2% bond length alternation). Although DFT calculations did not accurately reproduce experimentally determined or CCSD(T) singlet-triplet separation, both the local density approximation (LDA) [19] and the use of gradient-corrected (BLYP) [20] or hybrid (B3LYP) functionals gave relevant results in terms of geometries and harmonic frequencies [21]. Hund rule-reliable Lewis representations of small carbon chains are given in Scheme 1.2. With regard to the contribution of zwitterionic forms, it should be mentioned that a TD-LDA treatment showed that the longitudinal polarizability increases from approximately 7 Å^3 (n = 3) to approximately 490 Å^3 (n = 21), namely more rapidly than n, and more rapidly than the polarizability of the corresponding polyenes with the same number of valence electrons [18].

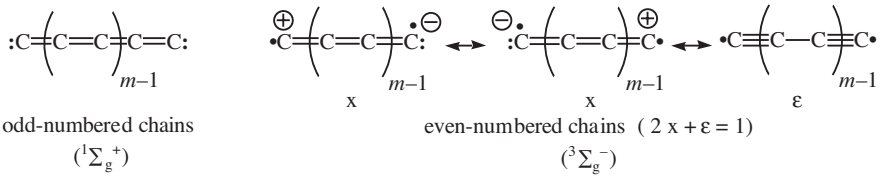

Scheme 1.2 Main Lewis forms for ground state C_{2m+1} and C_{2m} (m = 1–8) accounting for both the bond orders and the spin state.

Calculations of various excited or charged (C_n^-, C_n^+) states of linear carbon chains have been carried out at high levels of theory, especially by coupled cluster methods, which proved to be useful for reproduction or prediction of experimentally measured electronic spectra [22], electron affinities (EAs), ionization potentials (IPs), or dissociation energies (DEs) [17].

Efforts devoted to theoretical studies of linear carbon chains are motivated by their uniques properties, such as their role in fullerene growth or, more recently, in the field emission of electrons from carbon nanotubes or in the origin of the diffuse interstellar bands (DIBs) [18].

- C_n chains of nanometer sizes (n = 10–100) can be generated by electric field-induced unraveling of the inner graphene wall layers of carbon nanotubes, and are then responsible for emission currents of 0.1–1 μA under bias voltages of less than 80 V [23]. Indeed, linear C_n chains (n = 3–11) were calculated to pass relevant tests to qualify as metallic atomic wires with ease, but open-shell n-even chains give currents 100 times as intense as their closed-shell n-odd neighbors [19].
- A challenging goal in radio-astronomy is understanding of the origin of the DIBs, silent bands of frequency in the visible-IR spectra of interstellar clouds [22]. DIBs were previously proposed to be caused by linear carbon chains [24], and some of them could recently be identified with optical gas-phase electronic transitions of anionic representatives [25]. An alternative to the difficult experimental determination of the characteristics of such transitions is their calculation. A partial attempt using experimental energies and theoretical (TD-LDA) oscillator strengths of C_5–C_{21} carbon chains provided a few qualitative coincidences with observed DIBs [18].

The octet deficiency of carbon chains can be completed by closure to cyclo[n]carbons (see Section 1.3.2.4), by simple doping, by end-capping, or by passing from the molecular status to a material status through infinite expansion [26]. Whereas end-capping is the topic of the next section, doping can be exemplified by neutral and charged carbon clusters $[C_{2n}X]^q$, which have been studied at the DFT level when X is a main group metal atom [27]: the cyclic ω-diacetylide-type structures $\overline{C{\equiv}C\text{---}X\text{---}C{\equiv}C}$ are favored over the open-chain isomers for q = 0 and X divalent (e. g., X = Mg) [28], or for q = –1 and X monovalent (e. g., X = Na) [27]. Similar studies have been conducted with transition metal atoms, including with X = Pt at the B3LYP level [29].

Finally, infinite expansion affords carbyne (1D *sp* carbon allotrope), the missing link between atomic carbon and graphite (2D sp^2 carbon allotrope), which may be hybridized with the latter to design graphyne and related allotropic structures [30]. Although the carbon allotropes are beyond the scope of this chapter [31], it should be mentioned that several theoretical studies have focused on the possible structures and promising properties of these challenging materials [32].

1.2.3 Capped all-*sp* Oligoacetylenic Chains

1.2.3.1 all-*sp* Oligoacetylenic Chains between Redox-Silent Organic Groups

The recently surveyed state of the art of the characterization of doubly capped acetylenic chains $XC_{2n}Y$ prompted a comprehensive study of lower representatives (Scheme 1.3, $n \leq 6$) at various level of theory (HF, MP2, MP4, CCSD(T), B3P86, B3LYP, with various basis sets) [33a].

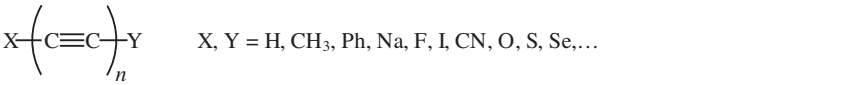

Scheme 1.3 Capped polyacetylenics.

For X = Y = H, let us first remind ourselves that the possible structures of small C_mH_2 molecules (m = 3, 5, 6, 7) have been investigated by various ab initio calculations (see, for example, refs. [33b–f]). For larger polyacetylenic representatives (m = $2n$, $n \leq 6$), geometrical, vibrational, and energetic (heats of formation, ionization potentials, electronic affinities (EAs)) properties display regular variations with respect to n [33a]. At the HF level, the C≡C and C–C bond lengths were found to converge to different values (1.190 Å and 1.366 Å, respectively), while the EAs decrease from 4.15 eV for n = 1 to 1.19 eV for n = 5. These results were extended by DFT studies of higher representatives (n = 6–12) [33]. The B3LYP level was argued to be relevant not only for the $^1\Sigma_g^+$ ground states of the neutral species, but also for the $^2\Pi_u$ or $^2\Pi_g$ ground states of the radical anions $[HC_{2n}H]^{\cdot -}$. In the latter, the bond length equalization increases with increasing n, while the adiabatic EAs of the neutral species increase continuously from 1.78 eV (n = 6) to 2.95 eV (n = 12). The number of calculated stretches in the 1900–2200 cm^{-1} region support the hypothesis that long $[HC_{2n}H]^q$ species (q = 0, –1, $n \geq 6$) could contribute to the DIBs [34]. It may be commented that the results from references [33a] and [34], though referring to different methods, could suggest that the EA is at its minimum around $n \approx 5$.

Chaquin et al. recently reported a comprehensive structural and vibrational study of the $HC_{2n}H$ molecules up to n = 20 at the B3LYP level [35]. The results confirm the persistency of bond length alternation with increasing n, and a systematic correlation scheme afforded asymptotic values of 1.229 Å and 1.329 Å for triple and single bonds, respectively. As would be expected, the asymptotic bond length alter-

nation (0.10 Å) is smaller than that obtained at the HF level (0.17 Å) [33a], but the DFT estimate is supported by excellent fits with experimentally obtained data. The alternation was also visualized through the ELF localization domains in $C_{30}H_2$ [35].

Polyynes have also received much attention, as they are predicted to exhibit large second hyperpolarizabilities [36]. Beyond ab initio calculations on simple diacetylene derivatives [36d–e], high level ab initio studies (SCF, MP, CCSD(T)) with large basis sets show that the static hyperpolarizability increases with increasing C≡C bond lengths [37]. The bond length alternation (BLA) parameter, which is a determining factor of nonlinear optical properties, was compared for polyyne chains at various calculation levels (PM3, ab initio, DFT) [38, 39]. The static second hyperpolarizabilities (γ of linear polyynes up to $C_{160}H_2$) was calculated [36b, 39] and, as in the case of polyenes, γ/n_C versus the number of carbon atoms n_C saturates beyond $n_C \approx 50$. Similarly, deprotonation and double deprotonation energies of polyynes containing up to 40 carbon atoms were shown to decrease towards an asymptotic limit of 370 kcal mol^{-1} [38b].

For X = Y = Ph (Scheme 1.3, $n \leq 6$), DFT studies of α,ω-diphenyl polyynes of D_{2h} symmetry accounted for the effects both of the chain length and of the phenyl endcaps on the fluorescence properties [40]. The fluorescent excited state switches from $1^1B_{2u}(\pi_x\pi_x^*)$ for $n \leq 2$ to 1^1A_u ($\pi_x\pi_y^*$ or $\pi_y\pi_x^*$) for $n \geq 3$.

For X = Y = O, S, Se, the acetylenic character is expected a priori for the triplet states (Scheme 1.3). The $OC_{2n}O$ molecules are much less stable than the cumulenic "odd" carbon suboxides $OC_{2n+1}O$. The first member of this series is ethylenedione C_2O_2 (i. e., the dimer of CO or the *carbo*-mer of O_2), which has hitherto evaded unambiguous experimental observation. On the basis of CCSD(T) calculations, it was recently suggested to be an intrinsically short-lived molecule [41]. The monosulfur analogue C_2OS [42] and the higher cumulogue C_4O_2 could, however, be identified by comparison between calculated and experimentally measured IR or UV spectra [43]. Recent calculations at the UB3LYP/6-311G* level support the view that all triplet structures $XC_{2n}X$ (X = O, S, Se; $n \leq 4$) possess a $^3\Sigma_g$ ground state with trivial spin contamination [44]. Both the C-C bond length alternation and the C-X bond lengths confirm the contribution of the acetylenic form $^{\bullet}X–(C\equiv C)_n–X^{\bullet}$.

For X, Y = H, CN (Scheme 1.3, $n \leq 9$), the corresponding cyanopolyynes H-$(C_2)_n$-CN and dicyanopolyynes NC-$(C_2)_n$-CN are regarded as isolable model substances of the carbyne allotrope [45]. The variation of the HOMO-LUMO gap (AM1, HF or MP2) and of the ZINDO-calculated UV spectra accounts for the experimentally observed Lewis–Calvin bathochromic shift with increasing n ($\lambda^2 = kn$). The observed regioselectivity of dienophile cycloadditions at the $C_\beta\equiv C_\gamma$ bonds is consistent with the highest positive Mulliken charges at the C_β and C_γ atoms (Scheme 1.4). Since the positive charge is greater at C_β than at C_γ, the weight of the long-range charge separation (y) is greater than that of the shorter-range one (x) (Scheme 1.4). The increase in cumulenic character with increasing n, also systematically evidenced at the B3LYP level [35], would thus be consistent with a parallel increase in the y/x ratio. The occurrence of the zwitterionic resonance forms would also account for the σ-coordination ability of the nitrogen atoms toward main group metals as evidenced by DFT calculations [46]. From a more applied

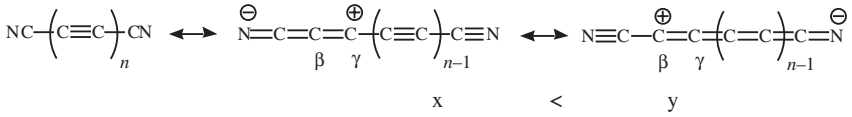

Scheme 1.4 Schematic charge separations in dicyanopolyynes.

standpoint, DFT-calculated low vibration frequencies of cyanopolyynes have also been claimed to be relevant for possible assignments of spectroscopic absorptions in interstellar media [35].

For X, Y = H, F, or Na (Scheme 1.3, $n \leq 5$), the electron distribution in the corresponding polyynes has been studied at the MP2/6-31G** level within the formalism of the electronegativity equalization method (EEM) [47]. In contrast to the atomic charges, the charges of the X-C≡C- and -C≡C-Y termini and those of the (n–2) intermediate -C≡C- units were found to be additive. For example, given n = 5 and X, Y = Na, F, the charges of the i^{th} unit in the heteronuclear and homonuclear molecules are bound through: $[Q_i(FC_{10}F) + Q_i(NaC_{10}Na)] \approx [Q_i(NaC_{10}F) + Q_i(FC_{10}Na)]$. This gives support to the view of the C_2 units as "compact" building blocks (see Section 1.2.1).

Much weaker than conventional hydrogen bonds, intermolecular π…π or C–H…π interactions have been attracting increasing attention [48]. In particular, several ab initio and DFT studies have focused on the hydrogen bond-accepting ability of triple bonds [49]. The ab initio intermolecular potential for acetylene sliding perpendicularly along a polyyne (Figure 1.2) was calculated at the MP2 level and was used to refine an MMC (molecular mechanics for clusters) model potential for polyynes [50]. The T-shaped interaction energy of acetylene with the triple bond at the end of the chain reaches an asymptote of –372 cm^{-1}. As the acetylene molecule slides along the chain, the intermolecular potential is essentially flat with only small bumps (Figure 1.2) (acetylene interacts slightly more with the triple C≡C bonds than with the single C-C bonds). This extended smooth intermolecular potential zone produces weak bonding slipperiness of acetylene along the polyyne chain.

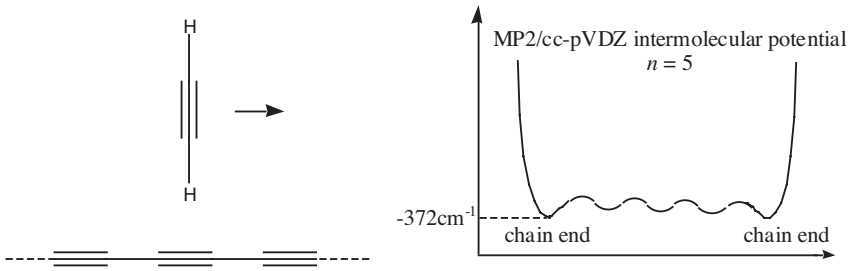

Figure 1.2 Perpendicular sliding of acetylene along a polyyne $H(C{\equiv}C)_nH$ (n = 2–5) at fixed distance between the center of mass of acetylene and the polyyne molecular axis (4.5 Å) [50].

1.2.3.2 All-*sp* Oligoacetylenic Chains between Organometallic Termini

Besides their potential applications in homogeneous and heterogeneous catalysis, alkynylmetal complexes are thermally robust, available in high yield, and attractive for their conducting and nonlinear optical properties. Among a very large number of theoretical studies on such complexes, a few recent results are highlighted below.

In monometallic complexes, theoretical studies have aimed at better understanding of metal-alkynyl bonding [51]. Through the use of the ADF program and the bond energy decomposition scheme designed by Ziegler and Rauk [52], metal-to-ligand backbonding energies were calculated for a set of σ-acetylide complexes of electron-rich metal centers such as $M(X)(PH_3)_n$, with M = Fe, Ru, Os (X = Cl and n = 4, or X = C_5H_5 and n = 2) [53, 54]. As expected, the π backbonding increases with the electron-withdrawing ability of the η^1-acetylide substituent and increases from Fe to Os. However, π bonding effects are relatively small in relation to the dominant metal-alkyne σ bonding. The backbonding energy is accurately correlated with the experimentally determined or calculated quadratic hyperpolarizability [55], but not with the υ(MC≡C) IR stretching frequency, which is indeed lowered by coupling with the stretching of the adjacent bonds. A similar DFT study of the influence of terminal substituents on the π backbonding in metallacumulene complexes has also been reported [56].

Studies of the homo- and heterobimetallic complexes have focused on the electronic communication between the metal centers through the polyyne bridge (Scheme 1.5) [57, 58, 59].

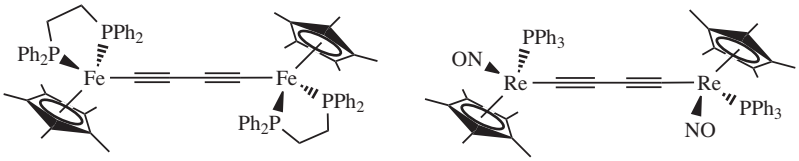

Scheme 1.5 Examples of homobimetallic complexes where electronic communication is assumed by polyyne bridges [64b].

In $L_mM{\cdots}C{\cdots}C{\cdots}ML_m$ complexes, the C_2 molecule (Section 1.2.1) is stabilized as a μ-diacetylide ligand [31, 60]. DFT calculations allow two classes of dicarbido complexes to be identified, the metals lying in pseudotetrahedral coordination spheres [61]. For early metals of the Ti, V, and Cr triads in high oxidation states with π-donor ligands, the coordination mode (M−C≡C−M, M=C=C=M, or M≡C–C≡M) depends on the d^n configuration. In contrast, for metals of the late triads (from Mn onwards) in low oxidation states with π-acceptor ligands, only the M−C≡C−M coordination mode is observed whatever the metal d^n configuration.

The generalized valence flexibility (M–C≡↔M=C=↔M≡C–) has been elegantly studied by natural bond order (NBO) and AIM analyses for even- [62] or odd-numbered [63] carbon chains, depending on the metallic end-caps. In the case of C_4 chains bonded to electron-rich metal fragments (M = Fe, Re, Ru,